

Retina-Choroid-Sclera Permeability for Ophthalmic Drugs in the Vitreous to Blood Direction: Quantitative Assessment

Nahid Haghjou · Mohammad J. Abdekhodaie · Yu-Ling Cheng

Received: 24 December 2011 / Accepted: 31 July 2012 / Published online: 2 October 2012
© Springer Science+Business Media, LLC 2012

ABSTRACT

Purpose To determine the outward permeability of retina-choroid-sclera (RCS) layer for different ophthalmic drugs and to develop correlations between drug physicochemical properties and RCS permeability.

Methods A finite volume model was developed to simulate pharmacokinetics in the eye following drug administration by intravitreal injection. The RCS permeability was determined for 32 compounds by best fitting the drug concentration-time profile obtained by simulation with previously reported experimental data. Multiple linear regression was then used to develop correlations between best fit RCS permeability and drugs physicochemical properties.

Results The RCS drug permeabilities had values that ranged over 3×10^{-6} m/s. Regression analysis for hydrophilic compounds showed that more than 92% of the variation in permeability values can be explained by correlative models of drug properties that include logarithm of the octanol-water partition coefficient (LogP), protein binding (PB), number of hydrogen bond acceptors (HBA), hydrogen bond donors (HBD), polar surface area (PSA) and dissociation constant (pKa) as independent variables. Regression analysis for lipophilic compounds showed that no significant correlation can be found between just physicochemical properties and RCS permeability.

Conclusion Using the RCS permeability obtained from this study for different drugs, one can predict pharmacokinetics of intravitreal drug delivery systems such as solid implants or colloidal systems. Furthermore, the developed correlations between RCS permeability and physicochemical properties of drugs are useful in early drug development by predicting RCS permeability and drug concentration in the vitreous without experimental data.

KEY WORDS computational fluid dynamic · intravitreal injection · ophthalmic drug · physicochemical properties · retina-choroid-sclera permeability

ABBREVIATIONS

AUC _{0-t}	area under the concentration-time curve
AUMC	area under the first moment concentration-time curve
CFD	computational fluid dynamic
HBA	hydrogen bond acceptors
HBD	hydrogen bond donors
HPLC	high performance liquid chromatography
K _{RCS}	permeability of retina-choroid-sclera membrane
LogDC	logarithm of distribution coefficient at pH 7
LogP	logarithm of the octanol-water partition coefficient of the neutral form
MRT	mean residence time
MW	molecular weight
MLR	multiple linear regression
PB	protein binding
pKa	ionization constant in water
PSA	polar surface area
RCS	retina-choroid-sclera membrane

INTRODUCTION

The aging of the general population, along with the higher incidences of eye diseases, such as age-related macular degeneration (AMD), diabetic retinopathy, endophthalmitis, retinitis pigmentosa (RP) or retinal edema, has created a need to deliver drugs to the posterior segment (*i.e.*, retina and choroid). Drug delivery to the posterior segment is a challenge as most drugs fail to reach therapeutic levels in this region after topical and systemic administration. It has generally been observed that drugs applied topically to the eye do not reach therapeutic levels in the posterior segment tissues, except perhaps by way of absorption from the pre-corneal area into the systemic circulation and redistribution

N. Haghjou · M. J. Abdekhodaie (✉)
Department of Chemical and Petroleum Engineering
Sharif University of Technology
Tehran, Iran
e-mail: abdmj@sharif.edu

M. J. Abdekhodaie · Y.-L. Cheng
Department of Chemical Engineering and Applied Chemistry
University of Toronto
Toronto, Ontario, Canada

into the retina/choroid (1). Most of the drug is cleared by the aqueous humor flow and fails to reach a therapeutic level near the retina. Systemic injections of drugs also yield low drug concentrations in the eye (2). Intravitreal injection is the most common approach used to deliver posterior levels of drugs in humans. It offers two major advantages over systemic therapy. First, it bypasses the blood-ocular barriers, allowing higher intraocular drug levels than could be achieved by systemic or topical administration. Second, it avoids many of the side effects associated with systemic therapy.

The duration of effects of an intravitreally administered drug depends on the retention of the injected drug at the site of administration. Following intravitreal administration, drug distributes within the vitreous by two different processes: diffusion and convection. For small to moderately sized molecules, such as fluorescein, diffusion is the predominant mechanism of transvitreal transport (3). Simultaneous with drug distribution within the vitreous body, drug elimination from the vitreous *via* two pathways also occurs: a) *via* the retina-choroid-sclera (RCS layer); b) through the anterior hyaloid membrane into the posterior chamber and then elimination by aqueous drainage. Drugs eliminated predominantly through the aqueous route (path b) have longer half-lives (15–30 h) resulting in prolonged therapeutic concentrations in the posterior segment tissues in comparison to the drugs eliminated across the RCS (2–4 h) (4). Loss of compounds eliminated primarily across the RCS is fairly

rapid because the anterior bottleneck between the lens and ciliary body is replaced by the wide surface area of retina for elimination. Previous studies shows that some compounds, such as fluorescein (5) or dexamethasone (6) tend to exit mainly *via* the RCS (path a). On the other hand, other substances with poor retinal permeability, such as foscarnet, diffuse primarily through the hyaloid membrane into the posterior chamber and eventually into the anterior chamber (path b) (7). The rational development of intraocular drug delivery systems and dosing regimens for treating posterior segment diseases require the understanding of the clearance behaviour of drugs from the vitreous chamber. The route of elimination from vitreous body is primarily determined by the physicochemical properties of the drug molecules. However, there does not exist any systematic study to address the correlation between RCS permeability and physicochemical properties. A scientific understanding of the relationship between drug physicochemical properties and its elimination from the eye is essential for the development of therapeutic agents with desired intravitreal pharmacokinetic properties. *In vitro* values of RCS permeability can be determined by diffusion studies with isolated tissues (8) or by *in vitro* cell culture models (9). In addition to being laborious, such *in vitro* methods do not properly capture *in vivo* transport mechanisms such as active pumping. *In vivo* ocular pharmacokinetic studies are challenging, because several animals must be sacrificed for each time point in the

Fig. 1 Geometry of the rabbit eye.

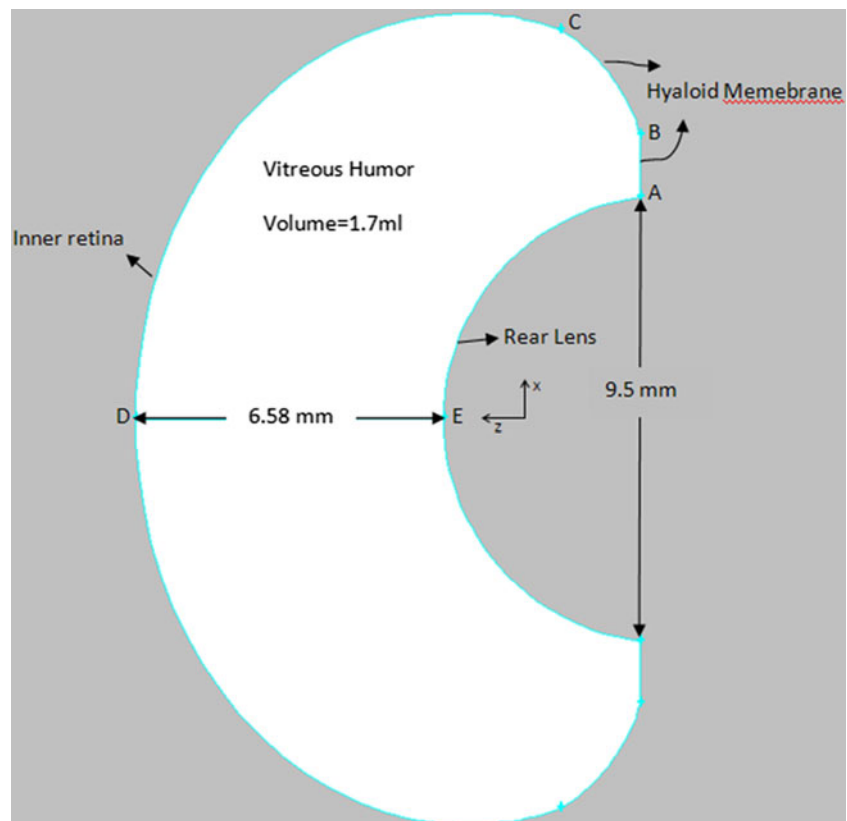


Table 1 Key Radii and Coordinates for the Rabbit Eye Model (Dimensions in cm)

	R1	R2	X	Z
Vitreous-retina boundary (inner retina- curve CD) ^a	0.8695857	0.7078275	0	0
Rear Lens (curve AE)	0.4786011		0	-0.4286011
Curved portion of hyaloid membrane (curve BC)	0.3836340		0.5067752	0
Intersection lens equator with hyaloid membrane (point A)			0.475	-0.37

^a The shape of the posterior segment is considered to be oval with radius R1 and R2

concentration-time curve. In the present work, a complementary method is presented that offers a way of predicting RCS permeability of drugs based only on drug properties. A CFD model combined with an optimization procedure was applied to calculate the RCS permeability of different drugs using previously reported experimental data of vitreous drug distribution after intravitreal injection in the rabbit eye; correlations between RCS permeability and drug physicochemical properties were then developed.

METHODS

CFD Model

In light of the importance of intravitreal drug distribution, several mathematical models and computer simulations have been developed to predict spatial-temporal distribution of drug in the vitreous (10–14). Some of these models are very detailed and require information regarding the diffusivity and partitioning of drug in various tissues surrounding the eye separately (*i.e.* retina, choroid and sclera), active pumping by RPE, choroidal loss and also loss to conjunctival lymphatics and episcleral veins. Since these data are not always available for different drugs, simpler models such as one developed by Friedrich and co-workers (11) which need fewer parameters are more applicable. In this study, a finite volume model has been used to find drug distribution in the vitreous humor of the rabbit eye after intravitreal injection. The physiological dimensions of the rabbit eye adapted in this study (Fig. 1) are in accordance with the model presented by Missel *et al.* (15). The rabbit eye was chosen because of available *in vivo* experimental data. Key dimensions of the model appear in Table 1. Because the vitreous is symmetrical and uniform about an axis that passes through the center of the lens and the vitreous, the 2D axis-symmetric geometry of the rabbit eye was generated. The vitreous chamber can be generated by rotating the model 360° about the axis. An unstructured mesh with 604 cells, 939 faces and 336 nodes are used in the computational domain.

Details of the computational model are provided in the Appendix I. In the present model, retina, choroid and sclera were considered as a single membrane (RCS membrane) with an average assigned permeability (K_{RCS}) for a specified drug. Drug clearance *via* the posterior rout is related to K_{RCS} as:

$$n(-D\nabla C + \vec{v}C) = K_{RCS} \times C \quad (1)$$

where, C is the concentration of the drug adjacent to RCS in the vitreous, D is the diffusion coefficient of drug in the vitreous, \vec{v} is the velocity vector of fluid flow. RCS permeability, K_{RCS} , which is the unknown parameter in the model, is one of the major determinants of the vitreous drug concentration profile. To determine the best-fit K_{RCS} , an initial guess for K_{RCS} was made based on the mean vitreal residence time of the drug (MRT). It is already known that the drugs with lower RCS permeability are cleared more slowly from the vitreous and therefore have higher MRT and *vice versa*. The optimum value of K_{RCS} was obtained by searching for the minimum of the objective function, which is defined as:

$$y = \sum_{t=t_i}^{t=t_f} \left(\frac{C_{exp,t} - C_t}{C_{exp,t}} \right)^2 \quad (2)$$

where $C_{exp,t}$ and C_t are the mean drug concentration in the vitreous at time t determined by experiment and simulation respectively. Nelder and Mead's simplex method which is, within reasonable limits, insensitive to a starting point was used in searching for the minimum of y . Previously reported experimental data of intravitreal injection of drugs in the New Zealand white (albino) rabbits was used to obtain the optimum value of K_{RCS} for each drug. Fig. 2 shows comparison of the

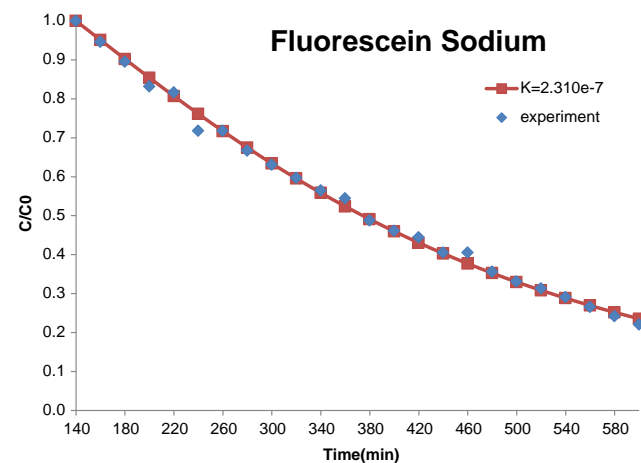


Fig. 2 Comparison of the predicted concentration-time profile of vitreous chamber following intravitreal administration of fluorescein with previously reported experimental results.

Table II Summary of Methods Used for Pharmacokinetic Studies of Intravitreal Injection in New Zealand White (Albino) Rabbits

No.	Compound	Injection Volume (μ L)	Vitreous Sampling Method	Assay Method	MRT (hr)	Duration of Experiment (hr)	Ref
1	Acyclovir	100	Implanted vitreous probe (Microdialysis)	HPLC	2.23	6	(32) ^a
2	Cefazolin	100	Implanted vitreous probe (Microdialysis)	HPLC	2.75	10	(33)
3	Ceftriaxone	100	Abel & Boyle method	well-diffusion microbiological assay	12.07	72	(16)
4	Cephalexin	100	Implanted vitreous probe (Microdialysis)	HPLC	3.13	10	(33)
5	Ciprofloxacin	100	Not mentioned	well-diffusion microbiological assay	4.17	8	(34)
6	Clarithromycin lactobionate	100	Freezing & dissecting the glob	HPLC	2.82	8	(35)
7	Cyclosporine A	20	Freezing & dissecting the glob	Scintillation counting	5.43	48	(36)
8	Floxacin	100	Not mentioned	well-diffusion microbiological assay	3.31	8	(34)
9	Fluorescein Sodium	100	Implanted vitreous probe (Microdialysis)	Reversed phase liquid chromatography	5.28	10	(37)
10	Ganciclovir	100	Implanted vitreous probe (Microdialysis)	HPLC	3.57	10	(38)
11	Grepafloxacin	100	Vitreous humor was aspirated	HPLC	4.29	24	(39)
12	Lincomycin	100	Freezing & dissecting the glob	Well Agar-Diffusion technique	12.47	72	(40)
13	L-phenylalanine	100	Implanted vitreous probe (Microdialysis)	Scintillation counting ($[^{14}\text{C}]\text{-L-Phe}$)	1.63	10	(41)
14	Methotrexate	32	Freezing & dissecting the glob	HPLC	8.41	48	(42)
15	Ofloxacin	100	Not mentioned	well-diffusion microbiological assay	3.29	8	(34)
16	Sparfloxacin	100	Not mentioned	well-diffusion microbiological assay	3.20	8	(34)
17	Vancomycin	100	Freezing & dissecting the glob	well-diffusion microbiological assay	15.82	42	(43) ^b
18	Voriconazole	100	Freezing & dissecting the glob	HPLC	4.22	48	(44)
19	I-Heptanol	100	Implanted vitreous probe (Microdialysis)	Not mentioned	2.62	10	(45)
20	I-Pentanol	100	Implanted vitreous probe (Microdialysis)	Not mentioned	2.07	7	(45)
21	I-Propanol	100	Implanted vitreous probe (Microdialysis)	Not mentioned	1.15	7	(45)
22	Methanol	100	Implanted vitreous probe (Microdialysis)	Not mentioned	0.98	7	(45)
23	FITC-Dextran	100	Microsampling	HPLC	3.61	10	(46)
24	FITC-Dextran	100	Microsampling	HPLC	4.14	10	(46)
25	FITC-Dextran	100	Microsampling	HPLC	4.69	10	(46)
26	Antiangiogenic Peptide(A6)	50	Freezing & dissecting the globe	Reversed-phase chromatography (XDB-Phenyl column)	36.51	336	(47)
27	Cidofovir	100	Freezing & dissecting the globe	HPLC	55.20	240	(48)
28	Foscarnet	100	Collecting vitreous from enucleated eye	HPLC	19.60	48	(49)
29	Gentamicin	100	Freezing & dissecting the globe	curve disk-plate assay using <i>Staphylococcus aureus</i> as the test organism	24.91	96	(50)

Table II (continued)

No.	Compound	Injection Volume (μL)	Vitreous Sampling Method	Assay Method	MRT (hr)	Duration of Experiment (hr)	Ref
30	ISIS2922 (Fomivirsen)	100	Freezing & dissecting the globe	anion exchange HPLC	80.94	480	(24)
31	Rituximab	100	Freezing & dissecting the globe	Immunoassay	160.72	408	(25)
32	Tobramycin	100	Aspiration of vitreous humor into a 5 ml-syringe	agar-diffusion bioassay using <i>Bacillus subtilis</i> as the test organism	39.21	192	(26)

^a The data for albino rabbits was used in the analysis

^b The data for uninfected rabbits was considered

predicted concentration–time profile of vitreous chamber following intravitreal injection of fluorescein with previously reported experimental results (37). The graphs for some other drugs are presented in the Appendix II.

The injection volume, vitreous sampling and assay method, mean residence time (MRT) in the vitreous chamber and duration of experiment for the selected drugs are summarized in Table II. MRT was calculated as follows:

$$MRT = \frac{AUMC}{AUC_{0-t}} \quad (3)$$

where AUC_{0-t} is area under the concentration-time curve and AUMC is area under the first moment concentration-time curve, both calculated by the trapezoidal rule:

$$AUC_{0-t} = \sum [(C_{n-1} + C_n)/2] [t_{n-1} + t_n] \quad (4)$$

$$AUMC = \sum [(C_{n-1}t_{n-1} + C_nt_n)/2] [t_{n-1} + t_n] \quad (5)$$

The optimum values of K_{RCS} for different drugs are listed in Table III.

Correlation Between RCS Permeability and Drug Properties

To find the correlation between RCS permeability and drug physicochemical properties, molecular descriptors were listed and independent variables were selected. Multiple linear regression analysis of independent variables was then performed to determine statistically significant relationships between the variables and RCS permeability.

Molecular Descriptors

Eight descriptors that are known to affect biomembranes permeability were selected for this study: molecular weight (MW), logarithm of the octanol-water partition coefficient of the neutral form of the drug (LogP), logarithm of distribution coefficient at pH 7 (LogDC), dissociation constant (pKa), protein binding (PB), number of hydrogen bond acceptors (HBA), number of hydrogen bond donor (HBD), and polar surface area (PSA). The values of these molecular descriptors for the listed compounds in Table III were collected from <http://www.drugbank.ca>. For some drug molecules, not all the physicochemical properties could be obtained and therefore they were not included in the statistical analysis.

Selection of Independent Variables

It is known from previous studies that lipophilic compounds prefer transcellular pathway while hydrophilic

Table III Physicochemical Properties and RCS Permeabilities of Various Soluble Drugs in New Zealand White (Albino) Rabbits

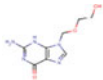
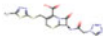
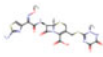
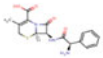
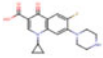
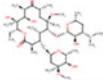

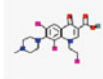
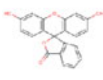
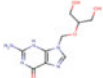
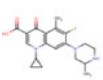
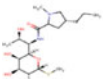
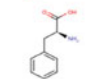
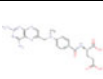
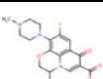
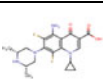
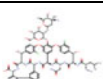
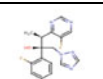

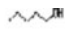
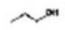
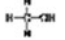
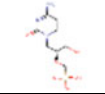
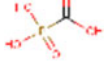
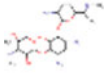
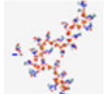

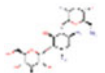
No. Compound	Formula	Chemical Structure	MW	pKa ^a	LogP ^a	LogDC ^b	PB(%) ^a	HBA ^a	HBD ^a	PSA(Å ²) ^a	K _{RCS} (m/s)
1	Acyclovir (Group I)		225.21	15.12	-1.56	-1.76	21.0	7	3	114.76	2.350E-06
2	Cefazolin (Group I)		454.5	10.87	-0.58	-2.53	80.0	9	2	156.09	1.860E-06
3	Ceftriaxone (Group I)		554.58	3.96	-1.7	-4	95.0	12	4	208.98	3.100E-08
4	Cephalexin (Group II)		347.39	4.5	0	-2.2	95.0	5	3	112.73	2.210E-06
5	Ciprofloxacin (Group II)		331.3	6.09	2.3	-0.85	30.0	6	2	72.88	3.905E-08
6	Clarithromycin Lactobionate (Group II)		747.95	8.99	1.7	1.98	70.0	13	4	182.91	1.700E-06
7	Cyclosporine A (Group II)		1202.61		2.92	3.4	90.0	12	5	279.00	2.402E-07
8	Fleroxacin (Group II)		369.34		0.24	0.91	32.0	9	1	64.10	1.430E-07
9	Fluorescein Sodium (Group II)		376.27	9.32	3.4	0.9	85.0	3	2	75.99	2.31E-07
10	Ganciclovir (Group I)		255.23	14.3	-1.7	-2.07	1.5	8	4	134.99	2.300E-06
11	Grepafloxacin (Group II)		359.39	carboxylate (7.1) amine (8.8)	2.9	0.07	50.0	6	2	72.88	2.290E-06
12	Lincomycin (Group II)		406.54	12.97	0.56	-0.85	72.5	7	5	122.49	2.500E-08
13	L-phenylalanine (Group I)		165.19	1.83 (carboxyl), 9.13 (amino)	-1.4	-3.53 ^c		3	2	63.32	2.702E-06
14	Methotrexate (Group I)		454.45	4.7	-2.2	-4.9	50.0	12	5	210.54	6.713E-08
15	Ofloxacin (Group II)		361.37	7.6	-2.1	-0.5	32.0	7	1	73.32	1.436E-07
16	Sparfloxacin (Group II)		392.4	15.89	2.5	0.94	45.0	7	3	98.90	1.760E-07
17	Vancomycin (Group I)		1449.25	8.78	-3.1	-4.7	55.0	24	19	530.49	5.517E-09
18	Voriconazole (Group II)		349.31		1	0.93	58.0	5	1	76.72	5.741E-07

Table III (continued)

No.	Compound	Formula	Chemical Structure	MW	pKa ^a	LogP ^a	LogDC ^b	PB(%) ^a	HBA ^a	HBD ^a	PSA (Å ²) ^a	K _{RCS} (m/s)
19	1-Heptanol (Group II)	C ₇ H ₁₆ O		116.2		2.47 ^b	2.47		1	1	20.20	1.743E-06
20	1-Pentanol (Group II)	C ₅ H ₁₂ O		88.15		1.41 ^b	1.41		1	1	20.20	3.210E-06
21	1-propanol (Group II)	C ₃ H ₈ O		60.1	16	0.34 ^b	0.34		1	1	20.20	3.520E-06
22	Menthanol (Group II)	CH ₄ O		32.04	15.2	-0.72 ^b	-0.72		1	1	20.20	4.010E-06
23	FITC-Dextran (Group II)			4004		3 ^b	0.4					1.170E-06
24	FITC-Dextran (Group II)			9300		3 ^b	0.4					8.700E-07
25	FITC-Dextran (Group II)			38900		3 ^b	-0.4					6.400E-07
26	Antiangiogenic Peptide(A6)	Acetyl-Lys-Pro-Ser-Ser- Pro-Pro-Glu-Glu-NH ₂		911								≈0
27	Cidofovir (Group I)	C ₈ H ₁₄ N ₃ O ₆ P		279.19	7.9	-3.37 ^b		6.0	8	4	145.680	≈0
28	Foscarnet (Group I)	Na ₃ CO ₅ P ₆ H ₂ O		300.1	3.5	-2.532 ^b		15.5	5	3	94.83	≈0
29	Gentamicin (Group I)	C ₂₁ H ₄₃ N ₅ O ₇		477.59	13.16	-1.89 ^b	-7.9	15.0	12	8	199.73	≈0
30	ISIS2922 (Fomivirsen)	C ₂₁₄ H ₂₇₇ N ₆₈ O ₁₂₀ P ₂₁ S ₂₁		7045.69					143	50	3040	≈0
31	Rituximab (Group I)	C ₆₄₁₆ H ₉₈₇₄ N ₁₆₈₈ O ₁₉₈₇ S ₄₄		143860		-0.414 ^b						≈0
32	Tobramycin (Group I)	C ₁₈ H ₃₇ N ₅ O ₉		467.51	13.13			<30	14	10	268.17	≈0

^a Data obtained from www.drugbank.ca^b From reference (28)^c Obtained using formula: $\log D = \log P - \log \left[1 + 10^{(PKa-pH)} \right]$

compounds are mainly transported *via* paracellular pathway (17). Since different mechanisms contribute in each of these two pathways, the data set was divided into two groups based of the lipophilicity/hydrophilicity of the drug. A measure of the lipid solubility of a drug is usually given by its octanol/water equilibrium partition coefficient. The partition coefficient (P) is determined by adding the drug to a mixture of equal volumes of octanol and water and shaking the mixture vigorously to promote partitioning of the drug into each phase. When equilibrium is attained, the phases are separated and assayed for drug. P is given by:

$$P = \frac{C_{\text{octanol}}}{C_{\text{water}}} \quad (6)$$

where C_{octanol} is concentration of drug in the octanol phase and C_{water} is concentration of drug in the water phase. Often, the logarithm of the partition coefficient of the drug is used (LogP). For a given drug, if Log P=0, there is equal distribution of the drug in both phases; if Log P>0, the drug is lipid soluble; if Log P<0, the drug is water soluble.

Based on this definition, the two distinct groups were constructed. Group I consisted of hydrophilic drugs (drugs with negative LogP), and Group II consisted of lipophilic drugs (drugs with positive LogP). Correlation matrix of all the predictor

Table IV Correlation Matrix of the Predictor Variables for Group I (Hydrophil Drugs)

		LogMW	LogP	LogDC	pKa	PB	HBA	HBD	PSA
LogMW	Pearson Correlation	1							
	Sig. (2-tailed)								
	N	8							
LogP	Pearson Correlation	-.696	1						
	Sig. (2-tailed)	.055							
	N	8	8						
LogDC	Pearson Correlation	-.787*	.730*	1					
	Sig. (2-tailed)	.021	.040						
	N	8	8	8					
pKa	Pearson Correlation	-.597	.430	.891**	1				
	Sig. (2-tailed)	.118	.288	.003					
	N	8	8	8	8				
PB	Pearson Correlation	.542	.157	-.503	-.737	1			
	Sig. (2-tailed)	.267	.766	.310	.094				
	N	6	6	6	6	6			
HBA	Pearson Correlation	.896**	-.831*	-.715*	-.476	.283	1		
	Sig. (2-tailed)	.003	.011	.046	.233	.587			
	N	8	8	8	8	6	8		
HBD	Pearson Correlation	.700	-.863**	-.580	-.256	.035	.917**	1	
	Sig. (2-tailed)	.053	.006	.132	.540	.948	.001		
	N	8	8	8	8	6	8	8	
PSA	Pearson Correlation	.844**	-.839**	-.687	-.420	.233	.988**	.964**	1
	Sig. (2-tailed)	.008	.009	.060	.301	.657	.000	.000	
	N								

* Correlation is significant at the 0.05 level (2-tailed)

** Correlation is significant at the 0.01 level (2-tailed)

variables for the two groups of drugs was formed (Tables IV and V). Multicollinearity condition that exists when independent variables are highly correlated with each other was tested. High values of correlation coefficients have been marked with an asterisk in Tables IV and V. Mathematically it is an ill-defined approach to use collinearly related parameters rather than independent parameters in multi-linear regression. Therefore, based on multicollinearity analysis, 2-parameter subsets of independent variables for both groups were constructed.

Furthermore, in order to better understand the importance of each physicochemical property, the linear correlation between the LogK_{RCS} and each of the eight variables for the two mentioned groups was determined (Table VI). The scatter plots of LogK_{RCS} versus significantly correlated variables of group I are shown in Fig. 3. For the purpose of comparison, the values of LogK_{RCS} for group II are also shown in Fig. 3.

Multiple Linear Regression Analysis

Multiple linear regression (MLR) models are useful: to understand which physicochemical properties have greatest

effect on the RCS permeability (K_{RCS}); to find the direction of the effects; and to predict RCS permeability for other drugs not listed in the table.

In order to determine statistically significant relationships between the independent variables and K_{RCS} , 2-parameter subsets of independent variables for both hydrophil and lipophil group were constructed. Then linear regression between LogK_{RCS} and the two independent parameters was performed and the best-fit models were obtained. A *P*-value of 0.05 or less was considered statistically significant. The various statistical parameters used to evaluate the model included coefficient of determination (R^2), adjusted R^2 , *F*-ratio and standard error (S.E). R^2 is an indicator of how well the model fits the data. Models with R^2 value of greater than 0.9 were selected in this study. Addition of variables to a regression equation improves R^2 even in the absence of significant predictive capability. The adjusted R^2 avoids this difficulty as it is adjusted for the degrees of freedom. Upon addition of variables to an equation, adjusted R^2 improves only if the new variables have an additional significant predictive capability. *F*-ratio is defined as the ratio of regression mean square and residual mean square.

Table V Correlation Matrix of the Predictor Variables for Group II (Lipophil Drugs)

		LogMW	LogP	LogDC	pKa	PB	HBA	HBD	PSA
LogMW	Pearson Correlation	1							
	Sig. (2-tailed)								
	N	18							
LogP	Pearson Correlation	.483*	1						
	Sig. (2-tailed)	.043							
	N	18	18						
LogDC	Pearson Correlation	-.075	.449	1					
	Sig. (2-tailed)	.769	.062						
	N	18	18	18					
pKa	Pearson Correlation	-.526	-.344	-.185	1				
	Sig. (2-tailed)	.079	.274	.566					
	N	12	12	12	12				
PB	Pearson Correlation	.614*	.280	.418	.095	1			
	Sig. (2-tailed)	.034	.377	.176	.782				
	N	12	12	12	11	12			
HBA	Pearson Correlation	.884**	-.003	.066	-.342	.322	1		
	Sig. (2-tailed)	.000	.992	.814	.277	.307			
	N	15	15	15	12	12	15		
HBD	Pearson Correlation	.670**	.103	.094	-.129	.458	.624*	1	
	Sig. (2-tailed)	.006	.714	.740	.688	.135	.013		
	N	15	15	15	12	12	15	15	
PSA	Pearson Correlation	.853**	.096	.144	-.379	.593*	.841**	.810**	1
	Sig. (2-tailed)	.000	.734	.608	.224	.042	.000	.000	
	N	15	15	15	12	12	15	15	15

* Correlation is significant at the 0.05 level (2-tailed)

** Correlation is significant at the 0.01 level (2-tailed)

RESULTS AND DISCUSSION

In order to determine K_{RCS} for different compounds, previously reported experimental data of concentration-time profiles of 32 intravitreally injected drugs/drug surrogates in the albino rabbit eye were used. A finite volume model was developed to predict the drug concentration in the vitreous after intravitreal injection. RCS permeability for various compounds was determined by minimizing the total difference

between experimental concentration and simulation predicted concentration at all time points (Table III). The fitted value of RCS permeability for fluorescein was consistent with previously experimental results such as Cunha-Vaz & Maurice (18) and Araie & Maurice (5).

Different physicochemical properties that seem to have influence on biological membrane permeability were listed and checked for multicollinearity. Since most of physicochemical properties selected as molecular descriptors are highly

Table VI Correlation Coefficients Between K_{RCS} and Each Physicochemical Property for Two Groups of Drugs

		LogMW	LogP	LogDC	pKa	PB	HBA	HBD	PSA
Log K_{RCS} (Group I)	Pearson Correlation	-.780*	.815*	.827*	.732*	-.489	-.899**	-.794*	-.880**
	Sig. (2-tailed)	.023	.014	.011	.039	.325	.002	.019	.004
	N	8	8	8	8	6	8	8	8
Log K_{RCS} (Group II)	Pearson Correlation	-.074	-.037	.181	0.004	-0.103	-.360	-.331	-.245
	Sig. (2-tailed)	.777	.887	.486	.991	.763	.206	.248	.399
	N	17	17	17	10	11	14	14	14

** Correlation is significant at the 0.01 level (2-tailed)

* Correlation is significant at the 0.05 level (2-tailed)

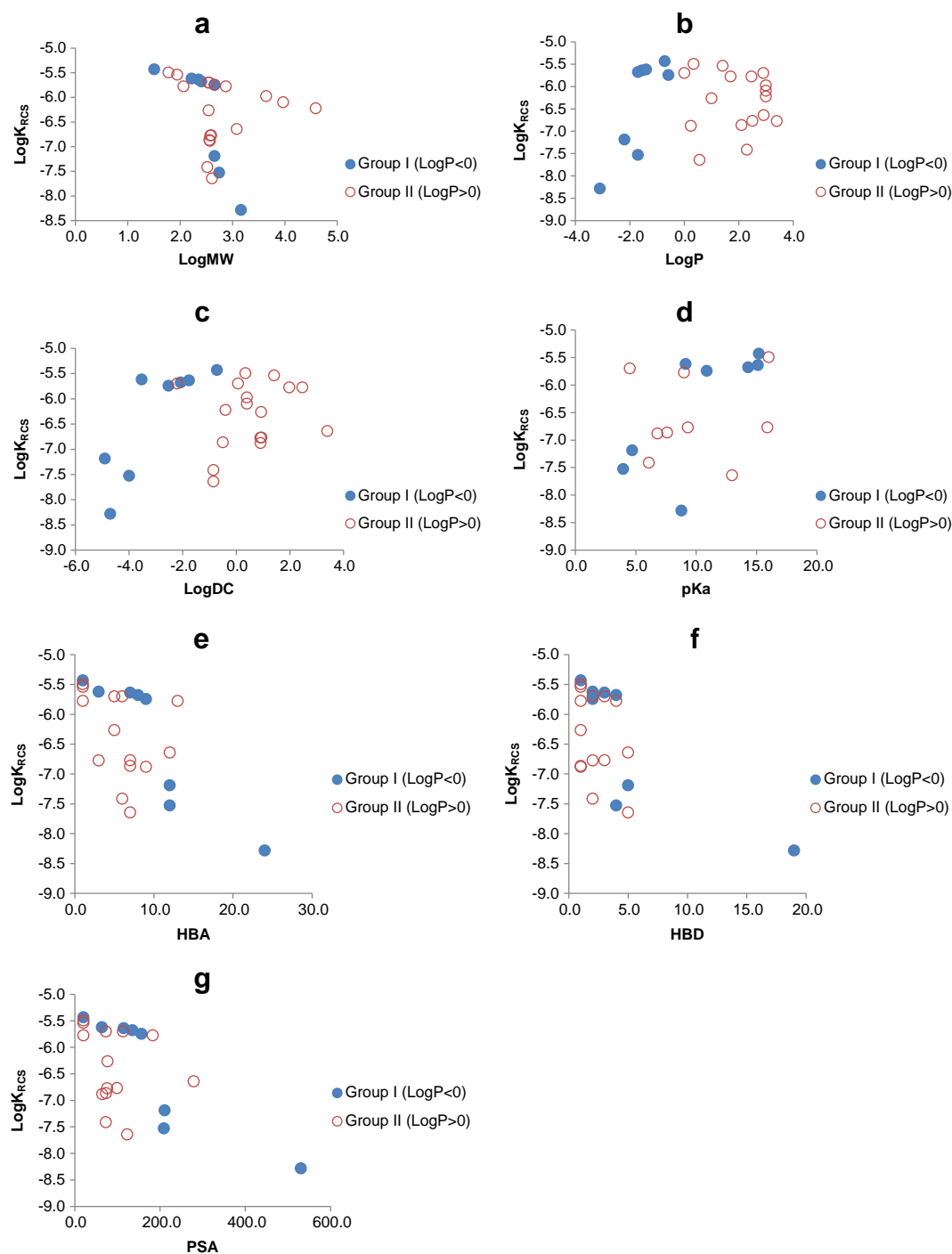


Fig. 3 Correlation between RCS permeability and physicochemical properties of drugs: (a) LogK_{RCS} vs. Log MW , (b) LogK_{RCS} vs. LogP , (c) LogK_{RCS} vs. LogDC , (d) LogK_{RCS} vs. pKa , (e) LogK_{RCS} vs. HBA , (f) LogK_{RCS} vs. HBD , (g) LogK_{RCS} vs. PSA .

correlated with each other, a model including all these properties as independent variables can't be interpreted correctly. Therefore 2-parameter sets of non-correlated variables for each group were constructed. The best-fit models were obtained from regression analysis of the different sets of independent variables for both groups. Considering a P-value of less than

0.05 and R^2 -value of greater than 0.9 for the models to be statistically significant, 4 models could be constructed for hydrophilic compounds (Group I, Table VII). For this group, LogP and PB were selected as the independent variables in the first model. In the second model pKa and HBA were used. In the third and fourth models HBA was replaced by HBD and

PSA respectively. Regression analysis showed that 99.4%, 92.7%, 92.9% and 93.4% of the variability in permeability data can be explained by models 1, 2, 3 and 4 respectively. The correlation between calculated RCS permeability based on best fitting with the experimental data (Table III) and model-predicted values based on the presented equations in Table VII are shown in Fig. 4. Good agreement was observed between calculated and predicted values of RCS permeability for all four models. In Group II, K_{RCS} showed no significant correlation with any of the specified sets of physicochemical properties. This can be attributed to difference in transport mechanisms of lipophilic and hydrophilic compounds. Across RCS barrier, drug can be transported *via* two routes : transcellular route and paracellular route. Lipophilic molecules have specialized transport processes and prefer the transcellular route, whereas hydrophilic molecules lacking membrane transport processes prefer the paracellular route. However, it is difficult to determine the fraction contributed by each pathway (19). The transport of most of the drugs is contributed by both pathways. Nine important mechanisms for drug transport and elimination from the RCS layer can be addressed as: 1) passive diffusion; 2) facilitated diffusion; 3) primary and secondary active transport; 4) transcytosis; 5) convective transport; 6) clearance *via* choroidal circulation; 7) binding to melanin; 8) loss to conjunctival lymphatics and episcleral veins; 9) drug metabolism (20). The mechanisms of transcellular transport include simple diffusion, facilitated diffusion, active transport, and endocytosis. Therefore, RCS permeability of lipophilic drugs can't be simply modelled by only physicochemical properties selected in this study.

The correlation coefficients (R values) between K_{RCS} and each physicochemical property for two groups of drugs are presented in Table VI.

Molecular weight (MW) which is often taken as the size descriptor of choice was negatively correlated with RCS permeability in Group I. This was predictable, because as mentioned before paracellular route is the main path for hydrophilic drugs and is mainly governed by the size and charge of the intercellular spaces and drug molecules (17). The correlation between LogMW and RCS permeability for Group II was much less significant because transcellular pathway is the predominant mechanism for transport of lipophilic drugs.

LogP which is octanol-water partition coefficient and is a measure of the lipid solubility of a drug is usually believed to be positively correlated to tissue permeability. Although LogP was positively correlated with Log K_{RCS} in Group I, it was negatively correlated with Log K_{RCS} in Group II. This can be explained by contribution of special transport mechanisms such as active transport.

Log DC, the logarithm of distribution coefficient of the drug at physiological pH, is usually employed instead of Log P as an estimation and/or prediction of absorptive potential. It is known that the ionized form of a molecule is more water-soluble and have negligible lipid solubility in comparison with the unionized form. Log DC is effectively the logarithm of the partition coefficient of the unionized form of the drug at a given pH. The relationship between the observed overall partition coefficient and the distribution coefficient is given by the below equation (21):

$$DC = P(1 - \alpha) \quad (7)$$

where α is the degree of ionization of drug. In Group I, LogDC was highly correlated with Log K_{RCS} . This trend is clearly indicated in the scatter plot shown in Fig. 3c. For Group II a linear correlation between Log K_{RCS} and LogDC was not observed. This plot suggests the existence of a sagittal relationship with maximum permeability around LogDC=2. This shows that although a degree of lipophilicity is necessary to enter the lipid membrane, compounds that are too lipophilic can be trapped in the membrane and never partition out again into the underlying aqueous environment.

HBA and HBD correlated negatively with Log K_{RCS} . The decreasing trend in RCS permeability with increasing the number of hydrogen bond acceptors and donors can be seen in Fig. 3e and f. Hydrogen bonds occur in presence of hydrophilic functional groups (*e.g.*, hydroxylic, carboxylic or amino groups). If a drug molecule forms hydrogen bonds with water, desolvation and breaking of the hydrogen bonds is required, prior to partitioning into the cell membrane. If the number of hydrogen bonds between the drug and water is high, too much energy is required and there will be minimal drug transport across the membrane, leading to longer residence time in the vitreous cavity.

Table VII The Best-Fit Equations for Prediction of RCS Permeability-Group I

Model	Best-fit equation ^{a,b}	R ²	Adj. R ²	F	S.E	Sig.
1	$\text{Log}K_{RCS} = -3.433(0.156) + 1.214(0.064)\text{LogP} - 0.020(0.002)\text{PB}$	0.994	0.989	235.393	0.117	0.001
2	$\text{Log}K_{RCS} = -6.303(0.498) + 0.098(0.034)\text{pKa} - 0.112(0.022)\text{HBA}$.927	.898	31.942	0.353	0.001
3	$\text{Log}K_{RCS} = -7.189(0.383) + 0.141(0.031)\text{pKa} - 0.124(0.024)\text{HBD}$	0.929	0.901	32.728	0.349	0.001
4	$\text{Log}K_{RCS} = -6.600(0.435) + 0.110(0.032)\text{pKa} - 0.005(0.001)\text{PSA}$.934	.907	35.286	0.337	0.001

^a Values in parenthesis indicate the standard error

^b All parameters used in equations are dimensionless except K_{RCS} (m/s) and PSA (\AA^2)

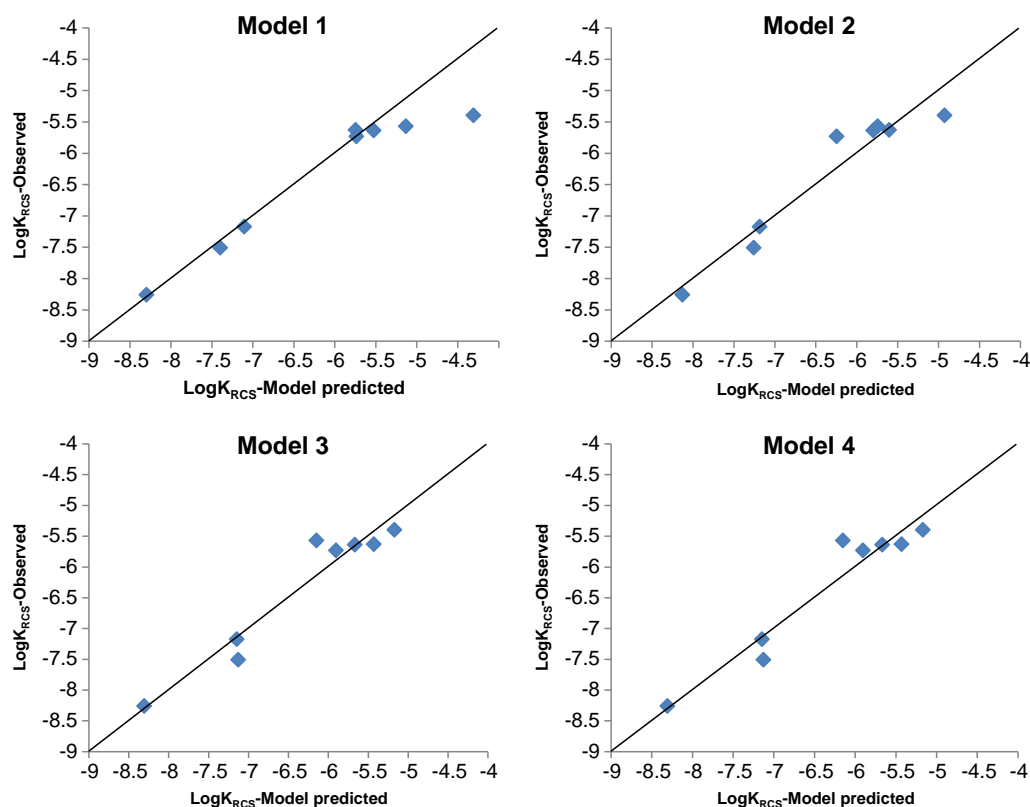


Fig. 4 Observed LogK_{RCS} (best fit of finite volume model to experimental data) versus Model predicted LogK_{RCS} (statistical correlation) according to 4 different models.

PSA, which is defined as the surface over all polar atoms, (usually oxygen and nitrogen), including also attached hydrogens, also negatively correlated with LogK_{RCS} in both groups. Fig. 3g shows a sigmoidal curve instead of a linear one for Group I and considerably more scatter for Group II. This is partly due to the fact that lipophilic compounds do not show only simple passive diffusion, but are also affected by active carriers and efflux mechanisms. Molecules with a polar surface area of greater than about 135 \AA^2 showed poor permeability in the RCS layer. This is consistent with previous studies investigating the effect of PSA on permeability of other tissues such as intestinal and brain (22,23).

CONCLUSION

In this study, first the outward RCS permeabilities (vitreous \rightarrow blood) for 32 compounds were calculated by best fitting the CFD model results with prior literature reports of concentration-time profile of intravitreally administered drugs in the Albino rabbit eyes. In the second step, the correlation between RCS permeability and physicochemical properties of drugs was analysed. It was found that molecular weight, lipophilicity or octanol-water partition

coefficient, ionization at physiological pH, hydrogen bonding capacity and polar surface area of a drug solute correlates reasonably well with RCS permeability. This is especially true for hydrophilic drugs whose main path is through paracellular spaces and passive diffusion is the predominant mechanism for their transport through the cell layers. Four predictive models were suggested for RCS permeability of hydrophilic compounds. The developed models are useful in the early phase of drug development when experimental data is not yet available. The RCS permeability predicted by these models could also be utilized to estimate drug concentration in the vitreous after drug administration by intravitreal injection or intravitreal drug delivery systems such as solid implants or colloidal systems.

Because of transcellular transport of lipophilic compounds, no statistically significant model could be obtained for this group if only drug physicochemical properties were considered. Clearly, in order to develop comprehensive models capable of predicting RCS permeation of both hydrophilic and lipophilic compounds, further studies are needed. These models could be useful in optimizing intravitreal dosing as well as designing drug delivery strategies in the treatment of posterior segment diseases.

ACKNOWLEDGMENTS AND DISCLOSURES

The authors wish to thank NSERC, 20/20 Ophthalmic Material Network of Canada for supporting this project and Dr. M.R. Pishvaie for his assistance.

APPENDIX I

CFD Model Construction

Governing Equations

Bulk flow through the vitreous body occurs due to the pressure gradient from the anterior part of the eye towards the posterior pole. This low level convective flow does not play any significant role for the distribution of low-molecular weight drugs. However, high-molecular weight drugs move through the vitreous as a result of bulk flow.

In order to evaluate the convective–diffusive drug transport within the eye, the fluid velocity was obtained by solving for creeping flow in a porous medium using Darcy's Law. According to Darcy's law, in laminar flows through porous media, the pressure drop is proportional to velocity as:

$$\vec{v} = -\left(\frac{K_h}{\mu}\right)_{vit} \nabla P \quad (\text{a1})$$

The aqueous humor is incompressible, hence:

$$\nabla \cdot \vec{v} = 0 \Rightarrow \left(\frac{K_h}{\mu}\right)_{vit} \nabla^2 P = 0 \quad (\text{a2})$$

where, \vec{v} is the velocity of the fluid, K_h is the hydraulic conductivity of the vitreous gel, μ is the viscosity of the fluid, P is the pressure, and ρ is the density. The flow is assumed to be steady and independent of the drug concentration.

To obtain the drug distribution, the species mass conservation equation was coupled with the flow field as:

$$\frac{\partial C}{\partial t} + \vec{v} \cdot \nabla C - D \nabla^2 C + q = 0 \quad (\text{a3})$$

where, C is the concentration of the drug, D is the diffusion coefficient of drug in the vitreous, and q is the generation/consumption rate of the drug. It is assumed that the drug is not metabolized or degraded within the vitreous, so q was set to zero.

Boundary Conditions

There are three main tissues that bound the vitreous humor: the hyaloid membrane, lens, and RCS layer. Boundary conditions are summarized in Table VIII.

Table VIII Summary of Boundary Conditions

Name	Momentum Eq.	Mass Transfer Eq.
Hyaloid Membrane	$P=2000 \text{ Pa}$	$n \cdot (-D \nabla C + \vec{v} C) = K_{hy} \times C$
RCS	$n \cdot \vec{v} = n \cdot \left[\left(\frac{K_h}{\mu} \right)_{RCS} \frac{P - P_v}{L} \right]$	$n \cdot (-D \nabla C + \vec{v} C) = K_{RCS} \times C$
Lens	$\vec{v} = 0$	$n \cdot (-D \nabla C + \vec{v} C) = 0$
Axis	$n \cdot \vec{v} = 0$	$\frac{\partial C}{\partial n} = 0$

The hyaloid membrane, which separates the vitreous humor from the anterior segment of the eye, is a suspensory ligament connecting lens and ciliary processes and is composed of loosely packed noncollagenous protein. Following Balachandran and Barocas (29), a flux boundary condition has been considered to represent the loss of the drug to the anterior segment. Assuming that the aqueous humor in the posterior chamber is well mixed, the flux of the drug at the hyaloid surface is expressed as:

$$n \cdot \left(-D \frac{\partial C}{\partial n} + \vec{v} C \right) = \frac{f}{A} \times C = k_{hy} \times C \quad (\text{a4})$$

Where f is the flow rate of aqueous humor [$3 \mu\text{l}/\text{min}$], A is the hyaloid membrane area (1.78 cm^2), and C is the concentration at the hyaloid surface.

Pressure at the hyaloid membrane is considered to be the same as that of aqueous humor, which is close to the intraocular pressure (IOP) of the eye. For a healthy eye, IOP is generally between 15 and 20 mmHg (2000–2666 Pa), whereas for a glaucomatous eye it can rise up to 40–80 mmHg (5333–10666 Pa) (30). In this study, pressure on hyaloid membrane is considered to be 15 mmHg (2000 Pa) for the normal eye.

The lens is assumed to be impermeable to both flow and the drug concentration. Therefore, at the surface of the lens a no-flux boundary condition for concentration and no slip boundary condition for flow have been applied.

The vitreous cavity is surrounded by several layers which give it mechanical support. Liquid leaving the vitreous chamber passes first through the retina, then the pigment epithelium, then through a loose capillary bed (the choroid and suprachoroid), then through the sclera, and finally through the loose episcleral tissue covering the eye. For the purpose of modelling, we have lumped the different tissues around the vitreous into one entity (RCS layer).

The boundary condition for momentum equation can be expressed by using Darcy's law as below:

$$\begin{aligned} n \cdot \vec{v} &= n \cdot \left[\left(-\frac{K_h}{\mu} \right)_{RCS} \nabla P \right] = n \cdot \left[\left(\frac{K_h}{\mu} \right)_{RCS} \frac{P - P_v}{L} \right] \\ &= K_p (P - P_v) \end{aligned} \quad (\text{a5})$$

where K_h is the hydraulic conductivity of RCS layer, μ is the aqueous humor viscosity, P is the pressure on the RCS layer adjacent to the vitreous, P_v is the pressure of the episcleral tissue (27) that is 9 mmHg (1200 Pa) and L is RCS thickness.

For the concentration boundary condition, both convective and diffusive transport of the drug from the vitreous to the retina has been considered. Various transport processes in RCS membrane control the movement of drug out of the vitreous chamber. The influence of all transport mechanisms out of the vitreous is incorporated in an unknown parameter which is referred to as RCS permeability, K_{RCS} , as:

$$n \cdot \left(-D \frac{\partial C}{\partial n} + \vec{v} C \right) = K_{RCS} \times C \quad (\text{a6})$$

Initial Condition

To model an intravitreal bolus injection of a specific value of drug, it is assumed that the drug is injected at the center of the vitreous chamber. This assumption is based on the method of injection used in all the previous pharmacokinetic experiments. The injected drug initially has a homogenous distribution within a spherical region. These assumptions are based on the injection method which was mentioned in related papers. The initial size of the spherical region is according to the volume of injected drug. The density of the drug solution is considered to be same as that of water *i.e.*, 1000 kg/m³. The initial normalized mass fraction of the drug is assumed to be 1 (normalized with respect to the concentration of the drug in the water base) within the domain of the drug injection site while it is 0 in rest of the vitreous. In mathematical words:

$$\begin{aligned} C_{t=0} &= 1 && \text{in the spherical drug source} \\ C_{t=0} &= 0 && \text{outside of the drug source} \end{aligned}$$

Model Parameters

The parameters required to solve the model are intraocular pressure (IOP), viscosity of the aqueous humor, hydraulic conductivity of the vitreous and RCS layer, drug diffusivity in the vitreous and RCS permeability. Of these parameters, two parameters depend on drug physicochemical properties and need to be calculated. These two parameters are drug vitreous diffusivity (D) and RCS layer permeability (K_{RCS}). The Stokes-Einstein equation was used to estimate drug vitreous diffusivity;

$$D = \frac{kT}{6\pi\eta r} \quad (\text{a7})$$

where k is the Boltzman Constant (1.38×10^{-23} J/K), T is the temperature, η is the viscosity of the solvent, and

r is the solute molecule radius which was calculated by:

$$r = \left[\frac{3(MW)}{4\pi N \rho} \right]^{\frac{1}{3}} \quad (\text{a8})$$

where MW is the solute molecular weight, N is the Avogadro's number and ρ is the density. Substituting Equation a8 into Stokes-Einstein equation gives:

$$D = \frac{kT}{6\pi\eta \left[\frac{3(MW)}{4\pi N \rho} \right]^{\frac{1}{3}}} \quad (\text{a9})$$

Therefore, drug diffusivity is inversely proportional to the cube-root of the molecular weight. The diffusivity of fluorescein in the vitreous humor has been found experimentally by Araie *et al.*(5) to be 6×10^{-10} m²/s. This value was used as base and vitreous diffusivity of other drugs was calculated as below:

$$D \cong 6 \times 10^{-10} \times \left(\frac{MW_{\text{fluorescein}}}{MW} \right)^{\frac{1}{3}} \quad (\text{a10})$$

For estimation of K_{RCS} , an initial guess for K_{RCS} was made based on the mean residence time of the drug in the vitreous. Later on the optimum value of K_{RCS} was obtained by minimizing the objective function y as described before.

The hydraulic conductivity of vitreous (K_h/μ)_{vit} and RCS membrane (K_p) were considered to be 8.4×10^{-11} m²/Pa.s and 5×10^{-12} m/Pa.s, respectively (31).

Computer Code

CFD calculations were conducted using FLUENT software version 12.1.4 (ANSYS, Inc., Canonsburg, PA). This code is based on a control volume approach where the computational domain is divided to a number of cells and the governing equations are discretized into algebraic equations in each cell. These equations satisfy the integral conservation of the mass and the momentum over each control

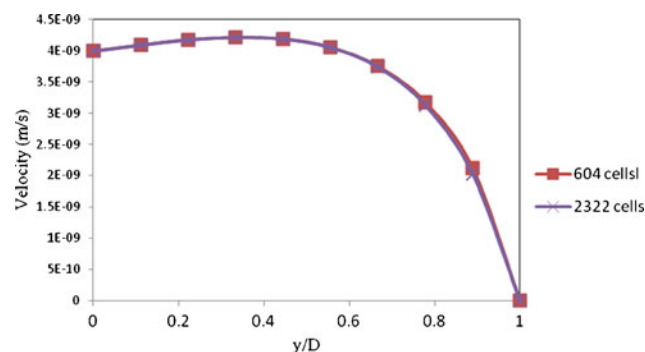
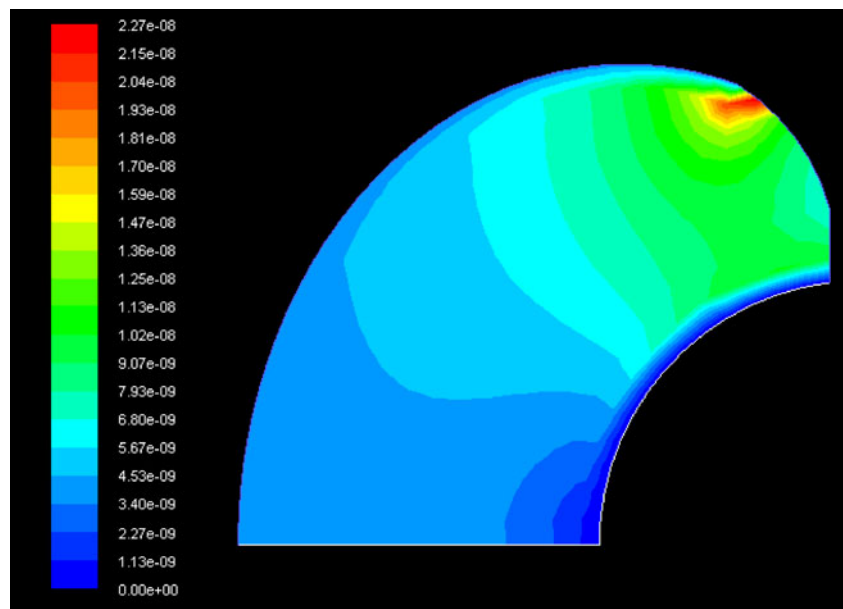


Fig. 5 Velocity magnitude along the center of vitreous chamber for 604 and 2322 cells.

Fig. 6 Contour plot of velocity magnitudes.



volume. Geometrical models and meshing were constructed using GAMBIT version 2.2.30.

Grid Independence Study

To check whether the size of grid is sufficient, grid size independence study has been done. A good grid size is one that has no influence on the results. When the grid is too fine numerical round off errors appear and when it is too coarse one could get truncation errors. Grid independence means that the converged solution obtained from a CFD calculation is independent of the grid density. As it is shown in Fig. 5 simulation with 604 cells and 2322 cells, creates less than 1.5%

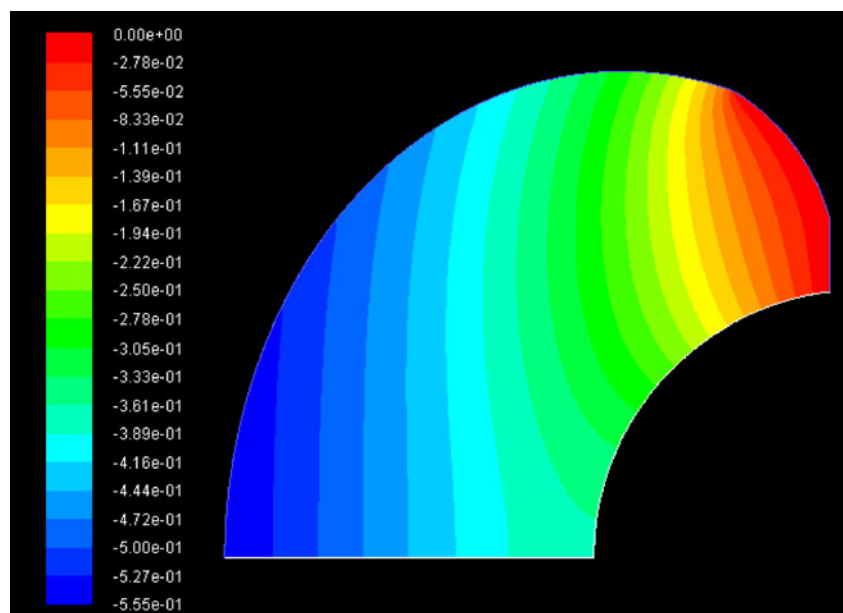
variation in the magnitude of velocity in the centreline of vitreous. This good agreement between the results from the two grid levels justifies the use of 604 cells for the simulation.

Velocity and Pressure Contour

Fig. 6 Shows the predicted fluid velocity contour within the vitreous chamber. The average velocity across the RCS surface was 4.0×10^{-9} m/s, and the average velocity in the vitreous was 7.12×10^{-9} m/s, which are consistent with earlier analysis (31).

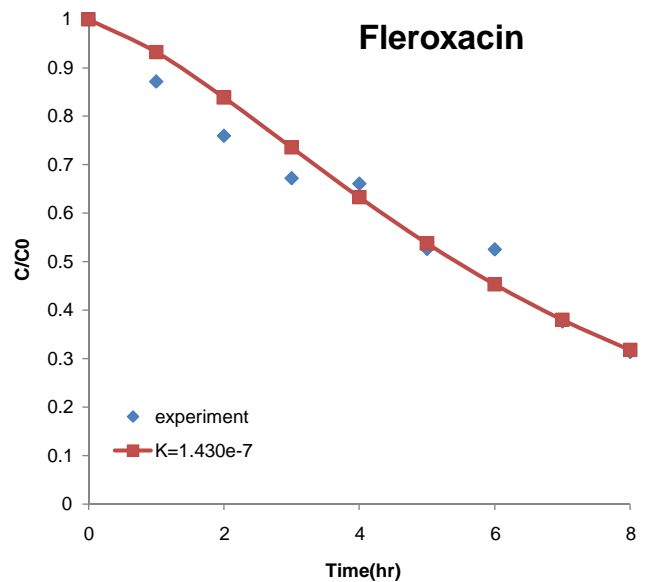
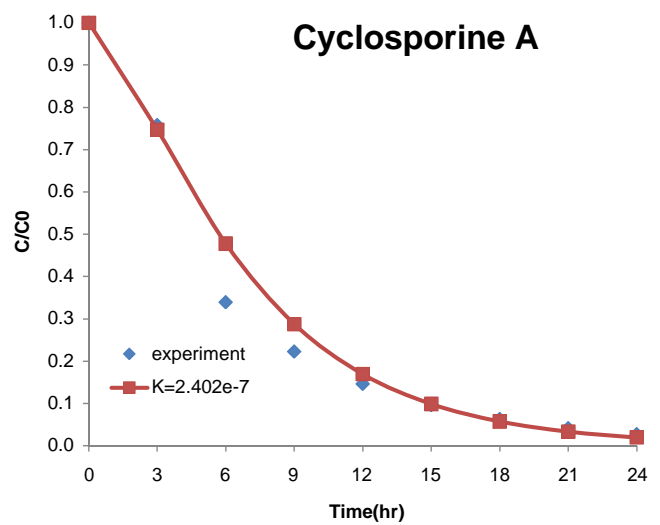
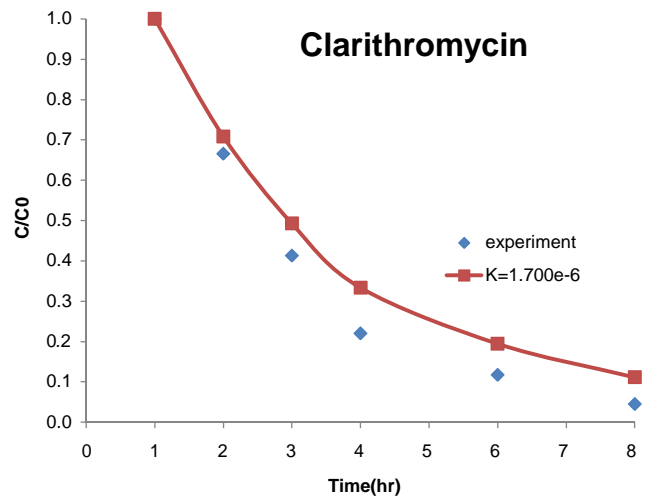
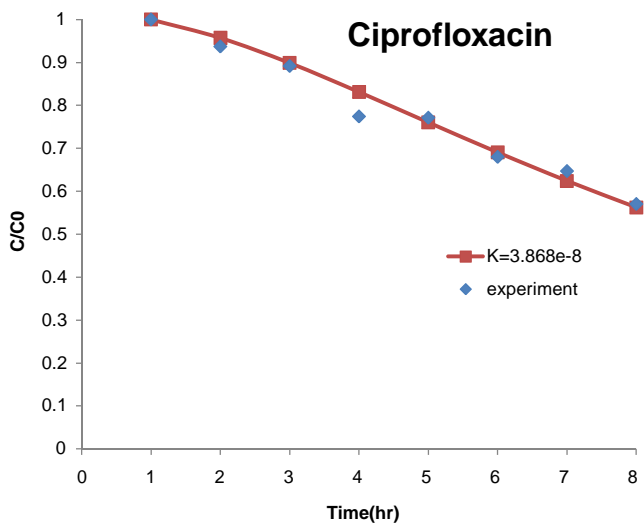
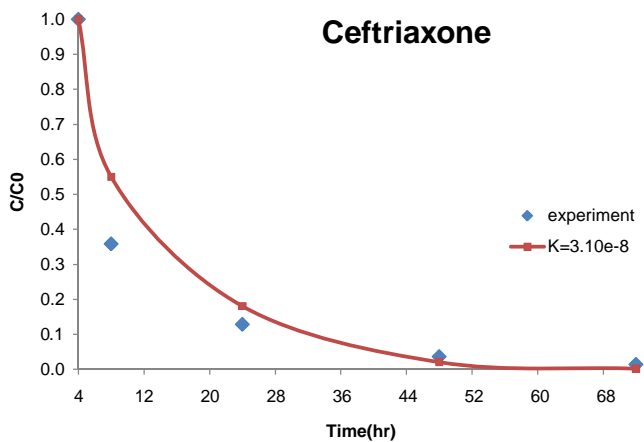
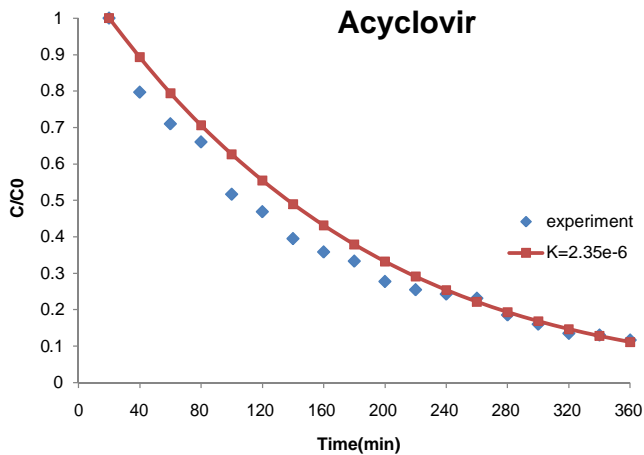
Fig. 7 Shows the pressure distribution within the vitreous. The higher pressure specified at the hyaloid membrane

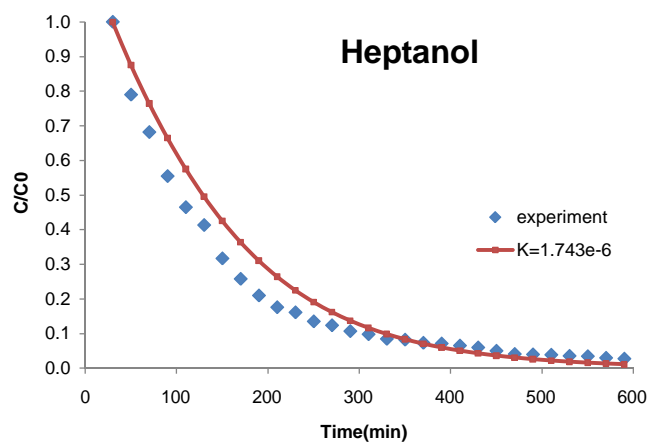
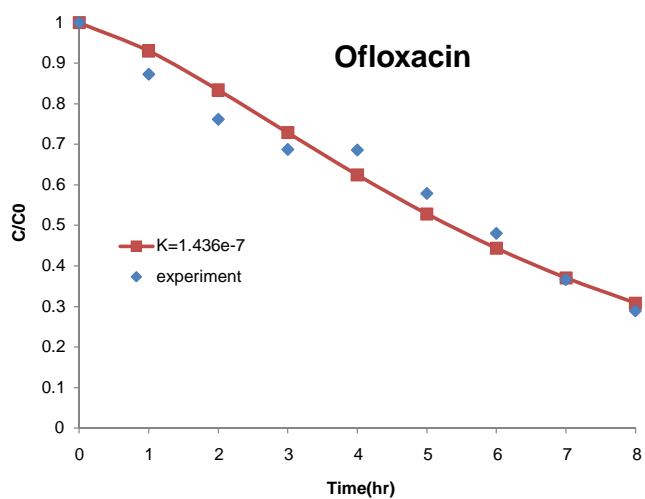
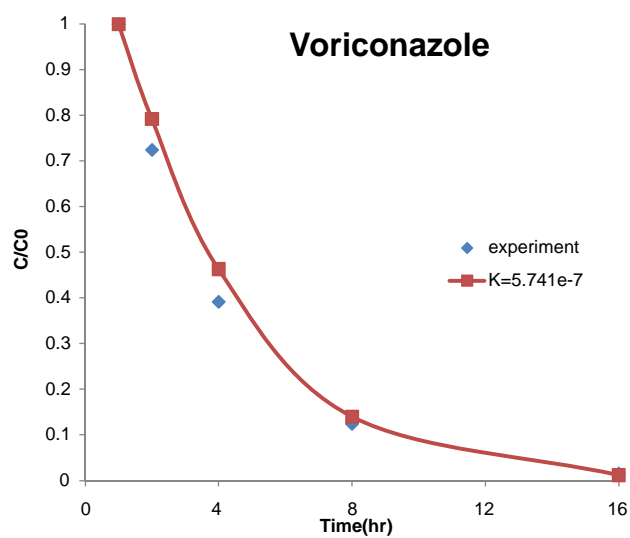
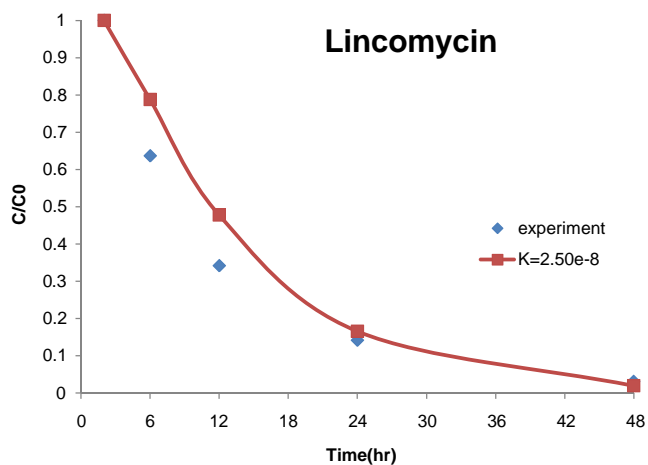
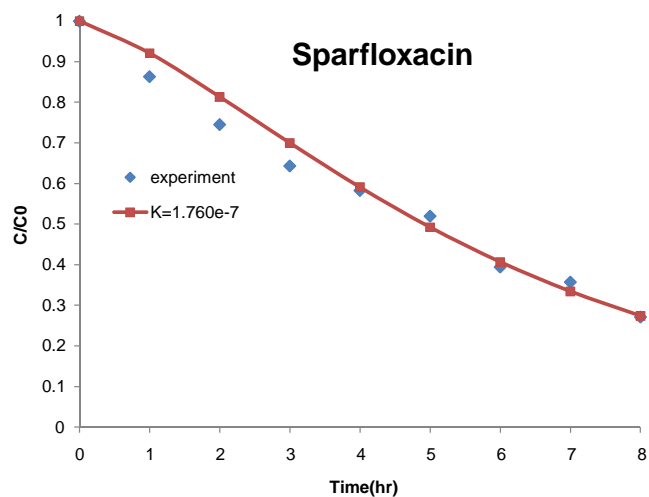
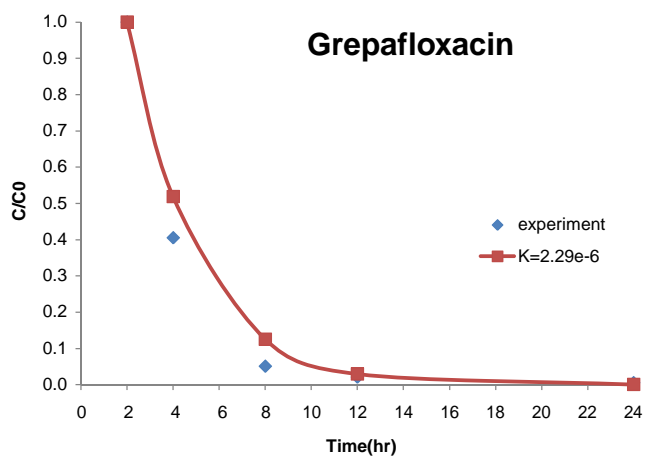
Fig. 7 Contour plot of pressure within vitreous (Pa) (pressure values are mentioned relative to the pressure at hyaloid membrane surface which is 2000 Pa).

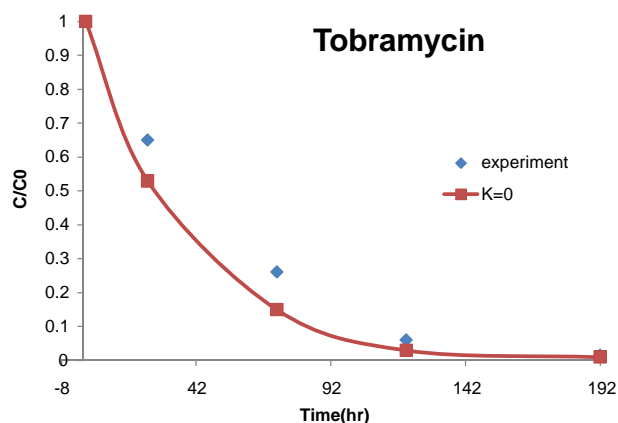
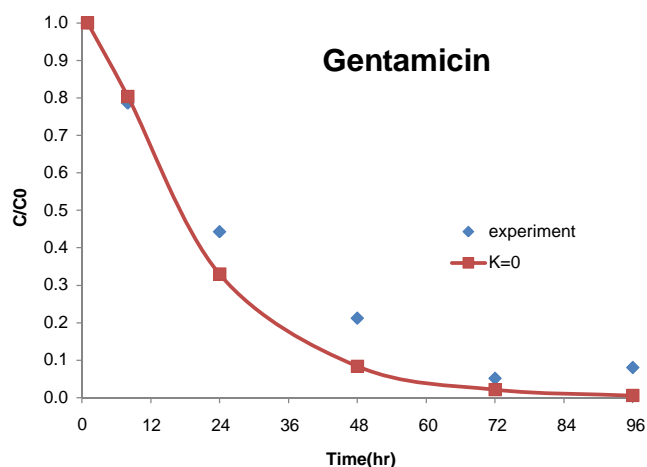


(15 mmHg=2000 Pa) drives the aqueous from the hyaloid to the outer sclera which is maintained at a venous pressure of 9 mmHg (1200 Pa). It is observed that the pressure drop across the vitreous is about 0.5 Pa (0.004 mmHg). Therefore, most of the pressure drop occurs in the RCS membrane.

APPENDIX II







REFERENCES

- Geroski DH, Edelhauser HF. Drug delivery for posterior segment eye disease. *Invest Ophthalmol Vis Sci.* 2000;41(5):961–4.
- Hughes PM, Olejnik O, Chang-Lin JE, Wilson CG. Topical and systemic drug delivery to the posterior segments. *Adv Drug Deliv Rev.* 2005;57:2010–32.
- Chastain JE. General considerations in ocular drug therapy. In: Mitra AK, editor. *Drug delivery systems*. New York: Marcel Dekker; 2003. p. 59–107.
- Maurice DM, Mishima S. Ocular pharmacokinetics. In: Sears ML, editor. *Pharmacology of the eye*. Berlin: Springer-Verlag; 1984. p. 19–116.
- Araie M, Maurice DM. The loss of fluorescein, fluorescein glucuronide and fluorescein isothiocyanate dextran from the vitreous by the anterior and retinal pathways. *Exp Eye Res.* 1991;52:27–39.
- Graham RO, Peyman GA. Intravitreal injection of dexamethasone: treatment of experimentally induced endophthalmitis. *Arch Ophthalmol.* 1974;92:149–54.
- Pitkänen L. Retinal pigment epithelium as a barrier in drug permeation and as a target of non-viral gene delivery, Ph.D. dissertation, University of Kuopio, 2007.
- Missel P, Chastain J, Mitra A, Kompella U, Kansara V, Duvvuri S, Amrite A, Cheruvu N. *In vitro* transport and partitioning of AL-4940, active metabolite of angiostatic agent anecortave acetate, in ocular tissues of the posterior segment. *J Ocul Pharmacol Ther.* 2010;26(2):137–45.
- Hornof M, Toropainen E, Urtti A. Cell culture models of the ocular barriers. *Eur J Pharm Biopharm.* 2005;60:207–25.
- Ohtori A, Tojo K. *In vivo/in vitro* correlation of intravitreal delivery of drugs with the help of computer simulation. *Biol Pharm Bull.* 1994;17:283–90.
- Friedrich S, Cheng YL, Saville B. Finite element modeling of drug distribution in the vitreous humor of the rabbit eye. *Ann Biomed Eng.* 1997;25:303–14.
- Missel PJ. Hydraulic flow and vascular clearance influences on intravitreal drug delivery. *Pharm Res.* 2002;19:1636–47.
- Missel PJ. Finite and infinitesimal representations of the vasculature: ocular drug clearance by vascular and hydraulic effects. *Ann Biomed Eng.* 2002;30:1128–39.
- Xu J, Heys JJ, Barocas VH, Randolph TW. Permeability and diffusion in vitreous humor: implications for drug delivery. *Pharm Res.* 2000;17:664–9.
- Missel PJ, Horner M, Muralikrishnan R. Simulating dissolution of intravitreal triamcinolone acetate suspensions in an anatomically accurate rabbit eye model. *Pharm Res.* 2010;27:1530–46.
- Shockey RK, Jay WM, Friberg TR, Aziz AM, Rissing JP, Aziz MZ. Intravitreal ceftriaxone in a rabbit model. Dose- and time-dependent toxic effects and pharmacokinetic analysis. *Arch Ophthalmol.* 1984;102:1236–8.
- Mäkiä A, Murtomäki L, Urtti A, Kontturi K. Drug permeation in biomembranes: *in vitro* and *in silico* prediction and influence of physicochemical properties. *Eur J Pharm Sci.* 2004;23:13–47.
- Cunha-Vaz JG, Maurice DM. The active transport of fluorescein by the retinal vessels and the retina. *J Physiol.* 1967;191:467–86.
- Ho NFH, Raub TJ, Burton PS, Barsutin CL, Adson A, Audus KL, Borchardt RT. Quantitative approaches to delineate passive transport mechanisms in cell culture monolayers. In: Amidon GL, Lee PI, Topp EM, editors. *Transport processes in pharmaceutical systems*. New York: Marcel Dekker; 1999. p. 219–316.
- Sunkara G, Kompella UB. Membrane transport processes in the eye. In: Mitra AK, editor. *Ophthalmic drug delivery systems*. New York: Marcel Dekker; 2003. p. 14.
- Hillery AM, Lloyd AW, Swarbrick J. Drug delivery and targeting for pharmacists and pharmaceutical scientists. Taylor & Francis; 2001. p. 21.
- Clark DE. Rapid calculation of polar molecular surface area and its application to the prediction of transport phenomena. 1. Prediction of intestinal absorption. *J Pharm Sci.* 1999;88:807–14.
- Van de Waterbeemd H, Smith DA, Beaumont K, Walker DK. Property-based design: optimisation of drug absorption and pharmacokinetics. *J Med Chem.* 2001;44:1313–33.
- Leeds JM, Henry SP, Truong L, Zutshi A, Levin AA, Kombrust D. Pharmacokinetics of a potential human cytomegalovirus therapeutic, a phosphorothioate oligonucleotide, after intravitreal injection in the rabbit. *Drug Metab Dispos.* 1997;25:921–6.
- Kim H, Csaky KG, Chan CC, Bungay PM, Lutz RJ, Dedrick RL, Yuan P, Rosenberg J, Grillo-Lopez AJ, Wilson WH, Robinson MR. The pharmacokinetics of rituximab following an intravitreal injection. *Exp Eye Res.* 2006;82:760–6.
- Kim EK, Kim HB. Pharmacokinetics of intravitreally injected liposome-encapsulated tobramycin in normal rabbits. *Yonsei Med J.* 1990;31:308–14.
- Blondeau P, Tetrault JP, Papamarkakis C. Diurnal variation of episcleral venous pressure in healthy patients: a pilot study. *J Glaucoma.* 2001;10:18–24.
- Durairaj C, Shah JC, Senapati S, Kompella UB. Prediction of vitreal half-life based on drug physicochemical properties: quantitative structure-pharmacokinetic relationships (QSPKR). *Pharm Res.* 2009;26:1236–60.

29. Balachandran RK, Barocas VH. Computer modelling of drug delivery to the posterior eye: effect of active transport and loss to choroidal blood flow. *Pharm Res*. 2008;25:2685–96.
30. Kaufman PL, Alm A. Adlers's physiology of the eye. 10th ed. Year book: Mosby; 2003.
31. Stay MS, Xu J, Randolph TW, Barocas VH. Computer simulation of convective and diffusive transport of controlled release drugs in the vitreous humor. *Pharmaceut Res*. 2003;20:96–102.
32. Hughes PM, Krishnamoorthy R, Mitra AK. Vitreous disposition of two acycloguanosine antivirals in the albino and pigmented rabbit models: a novel ocular microdialysis technique. *J Ocular Pharmacol Ther*. 1996;12:209–24.
33. Macha S, Mitra AK. Ocular pharmacokinetics of cephalosporins using microdialysis. *J Ocular Pharmacol Ther*. 2001;17:485–98.
34. Liu W, Liu QF, Perkins R, Drusano G, Louie A, Madu A, Mian U, Mayers M, Miller MH. Pharmacokinetics of sparflaxacin in the serum and vitreous humor of rabbits: physicochemical properties that regulate penetration of quinolone antimicrobials. *Antimicrob Agents Chemother*. 1998;42:1417–23.
35. Unal M, Peyman GA, Liang C, Hegazy H, Molinari LC, Chen J, Brun S, Tarcha PJ. Ocular toxicity of intravitreal clarithromycin. *Retina*. 1999;19:442–6.
36. Pearson PA, Jaffe GJ, Martin DF, Cordahi GJ, Grossniklaus H, Schmeisser ET, Ashton P. Evaluation of a delivery system providing long-term release of cyclosporine. *Arch Ophthalmol*. 1996;114:311–7.
37. Anand BS, Atluri H, Mitra AK. Validation of an ocular microdialysis technique in rabbits with permanently implanted vitreous probes: systemic and intravitreal pharmacokinetics of fluorescein. *Int J Pharm*. 2004;281:79–88.
38. Macha S, Mitra AK. Ocular disposition of ganciclovir and its monoester prodrugs following intravitreal administration using microdialysis. *Drug Metab Dispos*. 2002;30:670–5.
39. Solans C, Bregante MA, Garcia MA, Perez S. Ocular penetration of grepafloxacin after intravitreal administration in albino and pigmented rabbits. *Chemotherapy*. 2004;50:133–7.
40. Schenk G, Peyman GA. Lincomycin by direct intravitreal injection in the treatment of experimental bacterial endophthalmitis. *Albrecht Von Graefes Arch. Klin Exp Ophthalmol*. 1974;190:281–91.
41. Atluri H, Talluri RS, Mitra AK. Functional activity of a large neutral amino acid transporter (LAT) in rabbit retina: a study involving the *in vivo* retinal uptake and vitreal pharmacokinetics of l-phenyl alanine. *Int J Pharm*. 2008;347:23–30.
42. Velez G, Yuan P, Sung C, Tansey G, Reed GF, Chan CC, Nussenblatt RB, Robinson MR. Pharmacokinetics and toxicity of intravitreal chemotherapy for primary intraocular lymphoma. *Arch Ophthalmol*. 2001;119:1518–24.
43. Smith MA, Sorenson JA, Smith C, Miller M, Borenstein M. Effects of intravitreal dexamethasone on concentration of intravitreal vancomycin in experimental methicillin-resistant *Staphylococcus epidermidis* endophthalmitis. *Antimicrob Agents Chemother*. 1991;35:1298–302.
44. Shen YC, Wang MY, Wang CY, Tsai TC, Tsai HY, Lee YF, Wei LC. Clearance of intravitreal voriconazole. *Invest Ophthalmol Vis Sci*. 2007;48:2238–41.
45. Atluri H, Mitra AK. Disposition of short-chain aliphatic alcohols in rabbit vitreous by ocular microdialysis. *Exp Eye Res*. 2003;76:315–20.
46. Dias CS, Mitra AK. Vitreal elimination kinetics of large molecular weight FITC-labeled dextrans in albino rabbits using a novel microsampling technique. *J Pharm Sci*. 2000;89:572–8.
47. Koh HJ, Cheng L, Bessho K, Jones TR, Davidson MC, Freeman WR. Intraocular properties of urokinase-derived antiangiogenic A6 peptide in rabbits. *J Ocular Pharmacol Ther*. 2004;20:439–49.
48. Cundy KC, Lynch G, Shaw JP, Hitchcock MJ, Lee WA. Distribution and metabolism of intravitreal cidofovir and cyclic HPMP in rabbits. *Curr Eye Res*. 1996;15:569–76.
49. Berthe P, Baudouin C, Garraffo R, Hofmann P, Taburet AM, Lapalus P. Toxicologic and pharmacokinetic analysis of intravitreal injections of foscarnet, either alone or in combination with ganciclovir. *Invest Ophthalmol Vis Sci*. 1994;35:1038–45.
50. Peyman GA, May DR, Ericson ES, Apple D. Intraocular injection of gentamicin. Toxic effects of clearance. *Arch Ophthalmol*. 1974;92:42–7.